Evaluation of silicate minerals for pH control during bioremediation: Application to chlorinated solvents

Elsa Lacroix[a1], Alessandro Brovelli[a], Christof Holliger[b], D. A. Barry[a],

Ecole Polytechnique Fédérale de Lausanne (EPFL), School of Architecture, Civil and Environmental Engineering (ENAC), Lausanne, Switzerland

[a] *Ecological Engineering Laboratory*

[b] *Laboratory for Environmental Biotechnology*

Journal: *Water, Air and Soil Pollution*

[1] Author to whom all correspondence should be addressed. Tel. +41-21-69 34721; fax + 41-21-69 34722; e-mail elsa.lacroix@epfl.ch

Abstract

Accurate control of groundwater pH is of critical importance for *in situ* biological treatment of chlorinated solvents. This study evaluated a novel approach for buffering subsurface pH that relies on the use of silicate minerals as a long-term source of alkalinity. A screening methodology based on thermodynamic considerations and numerical simulations was developed to rank silicate minerals according to their buffering efficiency. A geochemical model including the main microbial processes driving groundwater acidification and silicate mineral dissolution was developed. Kinetic and thermodynamic data for silicate minerals dissolution were compiled. Results indicated that eight minerals (nepheline, fayalite, glaucophane, lizardite, grossular, almandine, cordierite and andradite) could potentially be used as buffering agents for the case considered. A sensitivity analysis was conducted to identify the dominant model parameters and processes. This showed that accurate characterization of mineral kinetic rate constants and solubility are crucial for reliable prediction of the acid-neutralizing capacity. In addition, the model can be used as a design tool to estimate the amount of mineral (total mass and specific surface area) required in field applications.

Keywords: groundwater acidification, *in situ* bioremediation, buffer injection, geochemical modeling, reductive dechlorination, organohalide respiration.

1 Introduction

Groundwater acidification of contaminated sites is a relatively frequent problem. The pH decrease can result from microbial processes (AFCEE 2004; Aulenta et al. 2006), presence of chemicals (like phenols or acid pesticides) and oxidative dissolution of sulfidic minerals, such as pyrite. Acidification is observed when the natural buffering capacity of ambient groundwater and soil is exceeded (McCarty et al. 2007; Robinson et al. 2009). Acidity buildup is of particular concern for *in situ* remediation processes such as bioremediation, chemical oxidation and reduction, and *in situ* mobilization-stabilization (Czupyrna 1989; ITRC 2005; Robinson et al. 2009). For example, if the pH is too low reaction rates may be reduced or the solubility of the target chemical may be too high or too low. Consequently, the application of such techniques is enhanced by implementation of efficient pH-control strategies.

In situ bioremediation of chlorinated aliphatic hydrocarbons (CAHs) is very sensitive to this issue (Adamson et al. 2004; Cope and Hughes 2001; McCarty et al. 2007). CAHs such as perchloroethylene (PCE) and trichloroethylene (TCE) are amongst the most frequently encountered subsurface contaminants due to their extensive use as dry cleaning and metal degreasing agents in many industrial processes (Fetzner 1998). CAHs are persistent in the environment and constitute a source of groundwater contamination that may last for decades (AFCEE 2004; McCarty et al. 2007). Enhanced *in situ* anaerobic bioremediation is a promising method to speed up their removal. It involves the stimulation of specialized anaerobic microorganisms that use chlorinated solvents as electron acceptors for energy metabolism through organohalide respiration (Yang and McCarty 2000, 2002). Stimulation of microbial activity is achieved by delivering an organic substrate into the subsurface, which is fermented to hydrogen, after which it is available as an electron donor for organohalide-

respiring bacteria (ORB) (AFCEE 2004). Organic substrate fermentation and organohalide respiration are both acid-producing processes, the extent of which is directly controlled by the amount of substrate and CAHs transformed (Adamson et al. 2004; AFCEE 2004; Amos et al. 2008; Chu et al. 2004). For this reason, source zone treatment is more susceptible to acidification than enhanced natural attenuation of dilute plumes due to the larger mass of CAHs available (Aulenta et al. 2006; Robinson et al. 2009).

Acidic conditions limit microbial degradation due to the inactivation of anaerobic bacteria at low pH. Pure strains of dehalogenating bacteria have a range of pH tolerance between 6 - 6.5 and 8 - 9.5 depending on the bacterial strain (Holliger et al. 1993; Krumholz 1997; Neumann et al. 1994; Scholz-Muramatsu et al. 1995; Sung et al. 2003; Suyama et al. 2001), while consortia are slightly more tolerant with a maximum pH range of 4 - 9 (Vainberg et al. 2009; Zhang and Bloom 1999). Fermenting bacteria exhibit a similar behavior with complete inhibition around pH 4 to 5 (Lee et al. 2002; Roychowdhury et al. 1988).

For field applications, the most common methods to control the pH decrease include the circulation of a solution containing dissolved alkaline materials (such as sodium or potassium bicarbonate) in the treatment zone (AFCEE 2004; Payne et al. 2006; Robinson et al. 2009) and the use of water injections to dilute the substrate and the acidity (Brovelli et al. 2011[2]) Constant addition of buffering agent requires frequent injections as alkalinity is rapidly consumed, which probably increases operation costs. In addition, in aquifers with significant concentrations of Ca^{2+} or Mg^{2+}, addition of bicarbonate may lead to precipitation of calcite at neutral pH (Lozecznik et al. 2010), which hinders further treatment.

[2] A. Brovelli, D. A. Barry, C. Robinson and J. I. Gerhard (2011). Analysis of acidity production during enhanced reductive dechlorination using a simplified reactive transport model. Submitted, Advances in Water Resources.

The aim of this work was to assess the feasibility of an alternative strategy for pH control, which relies on the use of silicate minerals. Silicate minerals are the most common rock-forming mineral and their weathering is the predominant buffering mechanism in sediments with negligible carbonate content (Appelo and Postma 2005). The dissolution of silicates is accompanied by a release of alkali cations (such as K^+, Na^+, and Mg^{2+}) and by consumption of protons. Both processes can increase groundwater pH. Silicate minerals are appealing buffering agents as

- Dissolution is slow compared with carbonates, and therefore they are long-term sources of alkalinity (Appelo and Postma 2005);
- The dissolution rate is pH-dependent, that is, minerals dissolve faster in acidic conditions (Marini 2007; White and Brantley 1995). This enhances their efficacy, as it allows a more rapid return to nearly neutral conditions while dechlorination is taking place, and increases their lifetime when the groundwater pH is in the neutral range;
- The solubility is also pH-dependent with a higher solubility at acidic pH and limited solubility at neutral pH.

In other words, when acidity is produced, minerals dissolve until a near-neutral pH is reached, then dissolution reduces due to thermodynamic constraints. This prevents the increase of groundwater pH in the alkaline range, which is as unfavorable to ORB as low pH.

Only a limited number of studies have evaluated the potential of silicate minerals as acid-neutralizing agents for water remediation. Silicate minerals resulting from industrial processes such as glass and ceramic production were considered, which contained sodium and potassium feldspars, nepheline and wollastonite (Fernandez-Caliani et al. 2008; Kleiv and Sandvik 2000; Likens et al. 2004). In all cases, significant buffering capacity was observed and it was concluded that these materials can be used to mitigate water acidity and precipitate/stabilize heavy metals both in the soil (Kleiv and Sandvik 2000) and streams

(Fernandez-Caliani et al. 2008; Likens et al. 2004), resulting, for example, from acid mine drainage leaching. The studies conducted so far are, however, limited in the number of minerals and geochemical conditions considered. The objective of this study was to consider a larger spectrum of silicate minerals for acid neutralization than previous work. To this end, a screening methodology for the selection of the most suitable minerals was developed. The methodology was applied to the specific case of *in situ* bioremediation of chlorinated solvents, but can be extended to any decontamination technology requiring near-neutral pH conditions.

2 Methods

Silicate dissolution is primarily a surface process, and its dissolution rate depends on the available specific reactive surface area (Appelo and Postma 2005; Marini 2007; White and Brantley 1995). Silicate minerals have different thermodynamic and kinetic characteristics and their dissolution rates vary over several orders of magnitude (Marini 2007). The methodology used to identify silicate minerals for pH control in the context of *in situ* bioremediation consists of three steps, (i) identification of silicate mineral kinetic parameters, (ii) pre-selection based on thermodynamic considerations and (iii) numerical simulations to quantify and compare the buffering efficiency of the selected minerals.

Twenty silicate minerals (Table 1) were used as the starting point for the application of the screening methodology described in this work. These minerals were selected because (i) detailed studies on their dissolution kinetics were available in the literature, and (ii) their thermodynamic parameters (solubility constant and enthalpy variation) were available and tabulated in existing geochemical databases. To limit the number of numerical simulations, silicate minerals with low reactivity, i.e., a slow dissolution rate in the acidic range (rate constant $< 10^{-12}$ mol m^{-2} s^{-1}) were excluded from the list.

2.1 Identification of kinetic parameters

The first step consists in determining the values of key parameters for mineral dissolution modeling, i.e., thermodynamic and kinetic parameters. Thermodynamic parameters – such as solubility constant K_D and standard enthalpy of the reaction at 25°C ΔH– can normally be found in thermodynamic databases such as THERMODDEM (Blanc et al. 2007) and MINTEQA2 (Allison et al. 1991) (Table 1), whereas kinetic rates were not readily available. For a given temperature and at conditions far from equilibrium, the dissolution rate of most silicates can be expressed by the empirical rate law (White and Brantley 1995):

$$r = k_{H^+}\left(10^{-pH}\right)^{-n_{H^+}} + k_W + k_{OH^-}\left(10^{-pH}\right)^{-n_{OH^-}}, \quad (1)$$

where r (mol m^{-2} s^{-1}) is the dissolution rate, k_H^+, k_W and k_{OH}^- (mol m^{-2} s^{-1}) are the rate constants for the acidic, neutral and alkaline ranges, and n_H^+ and n_{OH}^- are the reaction order of proton- and hydroxyl-promoted dissolution. Accurate determination of k_H^+, $k_{W,}$ k_{OH}^-, n_H^+ and n_{OH}^- is critical for geochemical modeling. In order to estimate these values, published data from mineral dissolution experiments were fitted with Eq. 1.

For each mineral, two datasets taken from the literature were considered. Only experiments conducted in similar conditions were adopted, i.e., measurements from flow-through reactors, far from equilibrium conditions and at a temperature of 25°C. Moreover, only experiments where steady state conditions were achieved were considered. The estimated parameters (Table 2) were compared with those reported by Palandri and Kharaka (2004).

2.2 Mineral screening based on thermodynamic considerations

Of the 20 silicate minerals selected, a first screening was performed considering solubility. This property depends on the solubility constant, K_D, and on the ion activity product, which is related to proton activity and therefore to pH. The dependency of solubility upon pH is

illustrated in Fig. 1 for five minerals (forsterite, wollastonite, nepheline, fayalite and andradite). Solubility is high in the acidic range and decreases by several orders of magnitude with increasing pH. The relationship, however, differs among minerals. For pH control in the context of *in situ* CAH bioremediation, a good buffering agent should have high solubility in the acidic range (pH 4-6) and low solubility in the neutral-basic range (pH 7-9). High solubility for acidic conditions results in a rapid return to neutral conditions while low solubility at high pH (> 7) prevents excessive basification of the groundwater. Solubility in pure water of the 20 selected minerals was computed at pH 5 and pH 8 at a temperature of 20°C using the geochemical code PHREEQC-2 (Parkhurst and Appelo 1999) and solubility constants from the MINTEQA2, THERMODDEM and LLNL thermodynamic databases (provided with PHREEQC-2). Minerals with low solubility at pH 5 (< 1 mmol l^{-1}) were excluded from the selection as they do not provide sufficient acid-neutralizing potential. Similarly, minerals with high solubility at pH 8 (above 10 mmol l^{-1}) were excluded, as they are likely to overshoot pH.

2.3 Numerical model

In order to estimate the acid-neutralization potential of silicate minerals, a batch numerical model was implemented using PHREEQC-2. The model included all relevant acid and alkalinity associated reactions occurring in chlorinated solvent-contaminated aquifers undergoing *in situ* bioremediation, i.e., mineral dissolution, microbial processes and chemical speciation. The model was run in batch mode to simulate a well-stirred reactor. In this work, transport was neglected as it was assumed that groundwater residence time is large compared to the time scale of geochemical reactions.

2.3.1 Acid-generating processes

Two microbial processes are primarily responsible for groundwater acidification during CAH bioremediation: fermentation of the soluble organic substrate and organohalide respiration (McCarty et al. 2007; Robinson et al. 2009). In most *in situ* bioremediation schemes, dissolved hydrogen gas, the electron donor for ORB, is delivered through fermentation of an organic substrate such as sodium lactate or linoleic acid,

$$\text{Organic substrate} + w H_2O = x CH_3COOH + y H_2 + z CO_2. \quad (2)$$

The right-hand side of this equation lists the fermentation products, i.e., hydrogen, acetic acid and carbon dioxide. The stoichiometric coefficients (*w*, *x*, *y*, *z*) are specific to the organic substrate used (Kouznetsova et al. 2010; McCarty et al. 2007; Robinson et al. 2009).

Not all hydrogen produced by fermentation is directed to organohalide respiration, as ORB must compete with other microbial guilds. In CAH source zones, sulfate and iron (III) are the two predominant competing terminal electron acceptors (AFCEE 2004; Aulenta et al. 2007). The fraction of hydrogen directed to ORB not only depends on the amount of iron oxides and sulfate present in the groundwater (AFCEE 2004), but also on microbial populations and specific field conditions and is therefore difficult to estimate precisely (Curtis 2003; Loffler et al. 1999). Following Robinson et al. (2009) and Robertson and Barry (2009), our model assumes that sulfate and iron oxide are present in excess in the system, and that a fraction f_{min} of hydrogen produced by fermentation is used by ORB.

Organohalide respiration, i.e., reduction of PCE to ethene is modeled as a sequential reaction involving four steps,

$$\text{PCE} \rightarrow \text{TCE} \qquad C_2Cl_4 + H_2 = C_2HCl_3 + HCl, \quad (3)$$

$$\text{TCE} \rightarrow \text{DCE} \qquad C_2HCl_3 + H_2 = C_2H_2Cl_2 + HCl, \quad (4)$$

DCE → VC $C_2H_2Cl_2 + H_2 = C_2H_3Cl + HCl,$ (5)

VC → Ethene $C_2H_3Cl + H_2 = C_2H_4 + HCl,$ (6)

where PCE stands for perchloroethylene, TCE for tetrachloroethylene, DCE for dichloroethene and VC for vinyl chloride. If the reaction completes, for each mole of PCE degraded four moles of hydrochloric acid are produced. The goal of the model is to simulate the rate at which acidity is produced and not all complex microbial processes. Therefore, in order to simplify the model and reduce the computational burden, the fermentation rate is not simulated directly. Instead, the fermentation reaction is combined with organohalide respiration to give the following overall dechlorination stoichiometry for each chloroethene (Robinson et al. 2009):

$$\text{Organic substrate} + \frac{w}{y\, f_{min}} H_2O + CAH_i = HCl + CAH_j + \frac{x}{y\, f_{min}} CH_3COOH + \frac{(1 - f_{min})}{f_{min}} H_2 + \frac{z}{y\, f_{min}} CO_2, \quad (7)$$

where CAH_i and CAH_j are the parent and daughter CAHs, respectively.

The following assumptions were made regarding the fermentative and organohalide respiring bacterial guilds:

1. Fermentation is inhibited by high level of hydrogen, as shown by Fennel and Gosset (1998). The fermentation rate is, therefore, controlled by hydrogen consumption by organohalide respiration and by other anaerobic respiration processes;
2. Acetate is not used as an electron donor. Robinson et al. (2009) demonstrated that acetate utilization as an electron donor lowers the overall acidity produced, so this represents the worst case in terms of acidity production;
3. The concentration of fermentative biomass is high and remains constant;
4. The impact of pH on microbial activity is similar for fermentative biomass and ORB;

5. Sufficient organic substrate is provided to ensure complete transformation of the PCE to ethene;
6. The organic substrate dissolution rate exceeds its fermentation rate.

Organohalide respiration rates were modeled using Monod-type kinetic equations including competitive and Haldane inhibition (Cupples et al. 2004; Yu and Semprini 2004). The degradation rate of each chloroethene was computed as

$$R_{\text{PCE reduction}} = \frac{k_{\max,\text{PCE}} X C_{\text{PCE}}}{K_{\text{S,PCE}} + C_{\text{PCE}}} f(\text{pH}), \tag{8}$$

$$R_{\text{TCE reduction}} = \frac{k_{\max,\text{TCE}} X C_{\text{TCE}}}{K_{\text{S,TCE}}\left(1+\frac{C_{\text{PCE}}}{K_{\text{CI,PCE}}}\right) + C_{\text{TCE}}\left(1+\frac{C_{\text{TCE}}}{K_{\text{HI,TCE}}}\right)} f(\text{pH}), \tag{9}$$

$$R_{\text{c-DCE reduction}} = \frac{k_{\max,\text{c-DCE}} X C_{\text{c-DCE}}}{K_{\text{S,DCE}}\left(1+\frac{C_{\text{TCE}}}{K_{\text{CI,TCE}}}\right) + C_{\text{DCE}}\left(1+\frac{C_{\text{c-DCE}}}{K_{\text{HI,c-DCE}}}\right)} f(\text{pH}), \tag{10}$$

$$R_{\text{VC reduction}} = \frac{k_{\max,\text{VC}} X C_{\text{VC}}}{K_{\text{S,VC}}\left(1+\frac{C_{\text{TCE}}}{K_{\text{CI,TCE}}}+\frac{C_{\text{c-DCE}}}{K_{\text{CI,c-DCE}}}\right) + C_{\text{VC}}\left(1+\frac{C_{\text{VC}}}{K_{\text{HI,VC}}}\right)} f(\text{pH}), \tag{11}$$

and their temporal dynamics is

$$\frac{dC_{\text{PCE}}}{dt} = R_{\text{PCE reduction}}, \tag{12}$$

$$\frac{dC_{\text{TCE}}}{dt} = R_{\text{PCE reduction}} - R_{\text{TCE reduction}}, \tag{13}$$

$$\frac{dC_{\text{c-DCE}}}{dt} = R_{\text{TCE reduction}} - R_{\text{c-DCE reduction}}, \tag{14}$$

$$\frac{dC_{\text{VC}}}{dt} = R_{\text{c-DCE reduction}} - R_{\text{VC reduction}}, \tag{15}$$

$$\frac{dC_{\text{ethene}}}{dt} = R_{\text{VC reduction}}, \tag{16}$$

where C_j (mol l^{-1}) is the aqueous concentration and $k_{max,j}$ (mol mg protein^{-1} d^{-1}) is the maximum specific utilization rate of CAH j (i.e., j = PCE, TCE, DCE, and VC), X (mg protein l^{-1}) the dechlorinating biomass concentration and K_S (mol l^{-1}) the half-saturation constant of each chloroethene, K_{CI} (mol l^{-1}) is the competitive inhibition constant and K_{HI} the Haldane inhibition constant. f(pH) is a pH inhibition function that is described in detail below (§2.3.2).

Microbial growth is expressed as:

$$\frac{dX}{dt} = -Y \sum_{i=1,5} R_{\text{j reduction}} - k_d X, \tag{12}$$

where X (mg protein l^{-1}) is the biomass concentration, Y (mg protein mol Cl released^{-1}) is the growth yield coefficient, $R_{\text{j reduction}}$ (mol l^{-1} d^{-1}) is the reduction rate of CAH j and k_d (d^{-1}) is the first-order biomass decay rate. It was assumed that all ORB populations have the same yield coefficient and decay rate.

2.3.2 pH inhibition function

ORB are highly sensitive to groundwater pH. The dechlorination rate is maximal in the near-neutral range and decreases in the acidic and basic ranges. Several pH inhibition functions have been proposed to describe the pH influence on microbial activity (Bailey and Ollis 1986; Lee et al. 2002; Mussati et al. 2005; Schepers et al. 2002). In this study, the Gaussian-type function employed by Schepers et al. (2002) was used:

$$f\left(\text{pH}\right) = \exp\left[-\frac{\left(\left|\text{pH}_{\text{opt}} - \text{pH}\right|\right)^n}{\sigma^2} \right], \tag{13}$$

where pH_{opt} (= 6.7) is the optimal pH, and n and σ are empirical parameters that were estimated by fitting published datasets (Vainberg et al. 2009) (Fig. 2).

2.3.3 Silicate mineral dissolution

Silicate mineral dissolution is a kinetically controlled process influenced by external factors such as temperature, pressure, pH, thermodynamic affinity and water composition (Appelo and Postma 2005; Marini 2007). The general form of the rate law for mineral dissolution far from equilibrium proposed by Lasaga (1995) was adopted here:

$$R_{\mathrm{D}} = r' \frac{A_0}{V} g(A)(1-\Omega), \tag{14}$$

where R_{D} (mol l^{-1}) is the mineral dissolution rate, r' (mol m^{-2} s^{-1}) is the rate per unit surface area (given by Eq. 15), A_0 (m^2) is the initial surface area, V (l) is the solution volume, Ω (-) the mineral saturation index, $g(A)$ (-) is a function which quantifies the changes in reactive surface area as dissolution proceeds.

The rate per unit surface area r' is a function of temperature, pH and groundwater composition and is expressed by:

$$r' = k_{\mathrm{H^+}} \frac{\left(10^{-\mathrm{pH}}\right)^{-n_{\mathrm{H^+}}}}{f_{\mathrm{H^+}}} \exp\left[-\frac{E_{\mathrm{H^+}}}{R}\left(\frac{1}{T}-\frac{1}{298}\right)\right] + \frac{k_{\mathrm{W}}}{f_W} \exp\left[-\frac{E_{\mathrm{W}}}{R}\left(\frac{1}{T}-\frac{1}{298}\right)\right] + k_{\mathrm{OH^-}} \left(10^{-\mathrm{pH}}\right)^{-n_{\mathrm{OH^-}}}, \tag{15}$$

where $E_{\mathrm{H}}{}^{+}$, E_{W} and $E_{\mathrm{OH}}{}^{-}$ (J mol^{-1}) are the activation energies for the acid, neutral and basic ranges, R (J K^{-1} mol^{-1}) the universal gas constant, T (K) the absolute temperature and $f_{\mathrm{H}}{}^{+}$ and f_{W} are factors accounting for inhibition by ionic species. The energy activation terms used in this study were taken from Palandri and Kharaka (2004) (Table 3). The effect of groundwater composition in the acidic and neutral ranges was included through the inhibition factors $f_{\mathrm{H}}{}^{+}$ and f_{W} (Appelo and Postma 2005):

$$f_{\mathrm{H^+}} = \left(1+\frac{[\mathrm{BC}]}{Lim_{\mathrm{BC,H^+}}}\right)^{x_{\mathrm{BC}}} + \left(1+\frac{[\mathrm{Al^{3+}}]}{Lim_{\mathrm{Al,H^+}}}\right)^{x_{\mathrm{Al}}}, \tag{16}$$

$$f_W = \left(1 + \frac{[BC]}{Lim_{BC,W}}\right)^{z_{BC}} + \left(1 + \frac{[Al^{3+}]}{Lim_{Al,W}}\right)^{z_{Al}}, \quad (17)$$

where *Lim* is the threshold activity for solute inhibition, [BC] indicates the sum of activities of the base cations Na^+, K^+ and Mg^{2+}, $[Al^{3+}]$ is the activity of aluminum and exponents x_i and z_i are empirical parameters. The effect of CO_2 on the dissolution rate was not included as it is negligible for partial pressures up to 1 bar (Golubev et al. 2005). The coefficients *Lim*, x_i and z_i were determined for a limited numbers of minerals by Sverdrup and Warfvinge (1995) and Sverdrup (1990), and were adopted in this work. For most minerals, however, these values were not available. As discussed in §3.4.5, the model is only slightly sensitive to these inhibition factors, and therefore they can be neglected in the conditions selected in this study.

The dissolution rate is also controlled by the available reactive surface area, which can change in time as the minerals dissolve (due, for example, to changes in the size and distribution of the crystal population, selective dissolution, aging of the mineral) (Appelo and Postma 2005). In addition, precipitation of secondary mineral phases may coat the surface of the dissolving mineral (Gaus et al. 2008; Scislewski and Zuddas). Reactive surface area is, however, not measurable. Also, it is difficult to correlate to the total surface area because, for instance, dissolution occurs only at certain sites on the mineral surface (Helgeson et al. 1984). Moreover, the reactive surface area might undergo variations of several orders of magnitude during dissolution (Brantley et al. 2008). Different models based on geometrical considerations have been proposed to relate changes in reactive surface area to mineral dissolution (Emmanuel and Berkowitz 2005; Kieffer et al. 1999; Lichtner 1988). In this study, the approach of Lichtner (1988) was adopted,

$$g(A) = \left(\frac{m}{m_0}\right)^{\alpha}, \quad (18)$$

where m_0 (mol) is the initial amount of mineral, m (mol) is the current amount of undissolved mineral and α is an exponent that depends on crystal shape, grain size distribution (Appelo and Postma 2005; Dixon and Hendrix 1993) and relative rates of dissolution on different surfaces (Witkamp et al. 1990). For a mono-disperse population of uniformly dissolving spheres or cubes α = 0.67, while α = 3.4 for a lognormal grain size distribution. Since this parameter is unknown and variable, α = 0.67 was arbitrarily chosen for the simulations conducted in this work and a sensitivity analysis was performed to assess its impact on model results.

Kinetic rate constants determined in laboratory experiments commonly exceed the mineral weathering rates observed in the field (White et al. 1996; White and Brantley 2003). Discrepancies were attributed to stirring in laboratory studies (Alkattan et al. 1998; Metz and Ganor 2001), inaccurate estimation of the mineral surface in aquifers (Brantley et al. 2008) and different characteristics of the mineral surfaces in the laboratory compared to field conditions (Davis and Hayes 1986). To correct dissolution rates obtained in the laboratory, following Vangrinsven and Vanriemsdijk (1992) a safety factor, *D*, was introduced,

$$R_D' = \frac{R_D}{D}, \tag{19}$$

where R_D (mol l^{-1}) is the total mineral dissolution rate obtained from continuous stirred flow reactor experiments and R_D' is the corrected value. Vangrinsven and Vanriemsdijk (1992) compared mineral dissolution rates in a number of different experiments and found $D \approx 15$ between dissolution rates determined in batch and in porous medium column experiments. This value was adopted in this work.

Precipitation of secondary minerals was not included due to the lack of a reliable modeling approach. Precipitation of a new mineral phase occurs when the saturation index exceeds a critical level, which is different for each mineral and in most cases is unknown (Zhu et al.

2010). Moreover, the definition of the initial surface area or of the nucleation sites is extremely difficult (Marini 2007; Zhu et al. 2010).

2.4 Numerical simulations

2.4.1 Definition of base conditions

The model developed above was set up to simulate conditions of a typical groundwater undergoing *in situ* bioremediation. The conditions used were:

- The groundwater composition was defined using major constituents of a typical site contaminated with chlorinated solvents: K^+, 0.2 mmol l^{-1}; Mg^{2+}, 2.3 mmol l^{-1}; Ca^{2+}, 7.2 mmol l^{-1}; Na^+, 5.9 mmol l^{-1}; Cl^- 0.2, mmol l^{-1}; SO_4^{2-}, 10.4 mmol l^{-1}; CO_3^{2-}, 5.1 mmol l^{-1}; pH, 6.8 (Kouznetsova et al. 2010);
- The temperature was set to 20°C: This value corresponds to the upper limit for groundwater temperature, which is usually between 10 and 20°C (AFCEE 2004). This value was chosen because microbial rates are much higher at 20°C than at 10°C (Holliger et al. 1993; Zhuang and Pavlostathis 1995), consequently so is acidity production. In other words, this is the worst-case condition in term of acidity production;
- The water was in equilibrium with a free phase of pure PCE (1.5 mmol l^{-1}). The solubility limit of PCE was set to 0.9 mmol l^{-1} (Yaws 1999);
- The factor f_{min} was set to 0.4, a typical value for field conditions (AFCEE 2004);
- The organic fermentable substrate used was linoleic acid, which is a major component of vegetable oil, a substrate often injected in field applications (AFCEE 2004). Linoleic acid is fermented to hydrogen and acetate following the reaction :

  $$C_{18}H_{32}O_2 + 16H_2O = 14H_2 + 9CH_3COOH; \quad (20)$$

- The microbial kinetic parameters (maximum specific utilization rates, half-saturation constants, competitive and Haldane inhibition constants) were taken from Yu and

Semprini (2004) for the PM culture, a mixed consortium able to convert PCE to ethene even at high PCE concentration. These kinetic parameters were determined at 20°C. All microbial processes model parameters used in the base case simulations are listed in Table 4;

- It was assumed that the natural buffering capacity of soil and groundwater was already consumed, again this is the worst-case scenario.

Three cases were considered:

Case A The pH was fixed at the optimal value for organohalide respiration (pH = 6.7). The goal was to determine the time needed to complete degradation without pH inhibition.

Case B This simulation was used to quantify the maximum dechlorination efficiency without addition of an external buffer.

Case C In this simulation, fayalite was added to the system. The goal was to ascertain the effect on pH and therefore on PCE degradation efficiency. A total of 10 g of mineral with a specific surface area of 30 m^2 g^{-1} were used, using the formula defined by Borkovec et al. (1993), which incorporates the effect of surface roughness. This corresponds to a powder with grain size around 1.5 μm.

Results were analyzed considering the time required converting 99% of the initial PCE mass to ethene ($t_{99\%}$). This metric is directly linked to the buffering effect as the only parameter influencing the dehalogenation rate is pH: A rapid dechlorination (high $t_{99\%}$) reflects a good buffering capacity of the mineral. $t_{99\%}$ of case C above (named $t_{BC,99\%}$) was used as a reference value in the sensitivity analysis.

2.4.2 Global sensitivity analysis

A global sensitivity analysis was conducted to ascertain the contribution of each parameter influencing mineral dissolution rate. This leads to identification of (i) insensitive parameters for model reduction and (ii) sensitive parameters that require a more accurate characterization. The analysis also improved the understanding of the model behavior and clarified the interactions among parameters. For each parameter considered, the range of variability found in the literature was used: the model was run using the two extreme values while keeping the other parameters fixed. The description of all the cases and the values of the parameters used for the simulation are given in Table 5. Cases 1 to 5 focus on the influence of the mineral dissolution kinetic parameters k_{H^+}, k_W, k_{OH^-}, n_{H^+}, n_{OH^-}, E_{H^+} and E_W. The importance of the security factor D was investigated in case 6. The influence of the thermodynamic parameters K_D and ΔH was evaluated in cases 7 and 8, respectively. To get a better understanding of the model behavior, some parameters were evaluated together, in particular the kinetic rate constants k_{H+} and k_W (case 2) and the energy activation terms, E_{H^+} and E_W (case 5). In addition to model parameters, simulations were run to ascertain the effect of other important variables. The effect of temperature was evaluated in case 9 where the model was run for 10 and 15°C. We considered also the inhibition of ionic species on mineral dissolution (case 10) and the representation of the reactive surface area changes (case 11). In this latter case, the parameter α was changed from 0.67 (uniform grain size distribution) to 3.4 (log normal distribution of the grains).

The $t_{s99\%}$ obtained from each run was compared to $t_{BC,99\%}$ and the difference $\Delta t_{99\%} = t_{s99\%} - t_{BC99\%}$ was computed. A high $\Delta t_{99\%}$ indicates a marked contribution of the parameter to the model output and vice-versa.

2.4.3 Mineral ranking

The acid neutralizing potential and lifetime of the minerals selected during the preliminary screening were also quantified, considering the $t_{99\%}$ metric and the mass of mineral consumed per mol of PCE degraded. For each mineral, the appropriate thermodynamic and kinetic data were included in the model and are listed in Tables 1, 2 and 3. The same amount of mineral (50 mmol l^{-1} and surface area of 300 m^2 of mineral l^{-1} of solution) was considered in all simulations. The results were used to rank the minerals according to their suitability for field application as buffering agents.

3 Results and Discussion

3.1 Determination of kinetic and thermodynamic parameters

Tables 1-3 report the results of the literature review conducted to collect the available kinetic and thermodynamic parameters for the 20 silicate minerals considered in this work. The stoichiometry of each dissolution reaction is also reported (Table 1), as it can be used to quantify the buffering potential of each mineral through the number of protons consumed per mole of dissolution. This value varies among the minerals, from 16 mol of protons per mole of dissolved mineral (cordierite, chlorite) to 2 moles of protons per mole of dissolved mineral (enstatite,wollastonite). Mineral dissolution kinetic parameters identified using Eq. 1 are listed in Table 2. For most minerals, the dissolution parameters in the alkaline range (k_{OH^-} and n_{OH^-}) could not be determined as most studies only considered the acid-neutral range. Even though the datasets considered were produced from experiments in similar conditions, large differences between them were found. These led to uncertainties in the determination of the parameters as large as 3 orders of magnitude for k_{H^+} and 2 orders of magnitude for k_W. These large ranges are likely due to one or more of the following: uncertainties in estimates of the available reactive surface area (Aagaard and Helgeson 1982; Gautier et al. 2001;

Helgeson et al. 1984), differences in the experimental design and solid phase preparation such as stirring rate (Metz and Ganor 2001), grinding method, or differences in the initial structure and composition of the mineral (Palandri and Kharaka 2004). When datasets for the same mineral were significantly different, a range of values was determined (Table 2). As an illustration, Fig. 3 shows the results of the fit for the mineral diopside. Two datasets were used (Golubev et al. 2005; Knauss et al. 1993) to determine the kinetic parameters. Fitting of the parameters was done for each dataset. As a result, two values were obtained for each parameter and the upper and lower limits of the kinetic equation were computed (Fig. 3).

All minerals considered have a pH-dependent dissolution rate with the reaction order of proton-promoted dissolution n_{H^+} between 0.14 and 1 (average value). Comparison of kinetic parameters showed high variability. In the acidic range, the kinetic constant k_{H^+} varies over 7 orders of magnitude, the fastest and slowest minerals being nepheline and albite. The kinetic constant in the neutral range k_W shows a slightly smaller variation (4 orders of magnitude between nepheline and albite).

The kinetic constants determined in this work fall in the range reported by Palandri and Kharaka (2004) for the majority of the minerals. A mismatch was found in seven cases, and was attributed to different criteria used to select the datasets. In particular, in contrast to the compilation of Palandri and Kharaka (2004), in this study only datasets using a similar experimental setup and conditions were considered.

3.2 Mineral screening based on thermodynamic considerations

The values of the solubility in the acid range at pH 5 and in the basic range at pH 8 are presented in Fig 4. Minerals with a solubility higher than 10 mmol l^{-1} are likely to lead to an increase of pH above 9, which is inhibitory to ORB (Vainberg et al. 2009; Zhuang and Pavlostathis 1995) and therefore they were excluded. On the other hand, in the acidic range

solubility should be sufficient to avoid limitation of mineral dissolution due to thermodynamic constraints. The minerals selected present a wide range of solubility at pH 5 and 20°C ranging from 4.3 mol l^{-1} for wollastonite to 8.45×10^{-5} mol l^{-1} for riebeckite. All minerals with solubility lower than 1 mmol l^{-1} were excluded. Minerals were classified in three classes according to their change in solubility as a function of pH (Table 6).

3.3 Base simulations

Base simulations demonstrated the positive impact of the addition of silicate mineral on groundwater pH and on the activity of ORB. If the influence of pH on dechlorination is neglected, degradation of 99% of 1.5 mmol l^{-1} of PCE to ethene occurs in 17 d ($t_{99\%}$) with transient accumulation of VC and to a smaller extent of DCE and TCE (Fig. 5a). Until day 2 the PCE concentration is equal to 0.9 mmol l^{-1} (PCE solubility). After 2 d, the separate PCE phase was dissolved and the aqueous PCE concentration started to decrease.

When the feedback of pH on ORB activity is considered, without an external source of alkalinity, the pH dropped below 4.5 after 9 d, stopping the dechlorination (Fig. 5b). Degradation of PCE was incomplete and, after 18 d, only 64% of the initial mass was transformed to DCE and VC. When dechlorination ceased, 4.6 mmol of acetate and 2.7 mmol of hydrochloric acid had been produced, indicating that the two processes contribute in a similar extent to groundwater acidification. This simulation highlights the need of an external buffer during enhanced bioremediation of CAHs when the natural soil buffering capacity is small.

The addition of fayalite had a positive impact on the CAHs degradation rates, with $t_{99\%}$ = 25 d (Fig. 5c). The pH initially dropped to 5.1 due to rapid conversion of PCE to VC because dechlorination was faster than mineral dissolution. Afterwards, the pH returned close to neutral as the transformation of VC to ethene is slower than the previous dechlorination steps

(see maximum degradation rates in Table 4) and because acidic conditions further reduced the activity of ORB. At the end of the simulation, 7 mmol of fayalite were consumed. When CAH removal was completed, the pH remained stable at 6.87 and mineral dissolution ceased since solubility of fayalite is very low at neutral pH (Fig. 1). This simulation suggested that, for the conditions considered, fayalite is a good candidate for groundwater buffering as pH remains close to neutral. Moreover, only the quantity required to buffer the acidity produced was used, and the rest remained in the system. This suggests that fayalite is also a good long-term source of alkalinity.

3.4 Global sensitivity analyses

3.4.1 Influence of mineral dissolution rate parameters

The results of the global sensitivity analysis are presented in the Table 5. The kinetic rate parameters in the alkaline range (k_{OH^-} and n_{OH^-}) have no influence on the degradation rate ($\Delta t_{99\%} = 0$) (cases 1 and 4). The reason is that water remains in the acid-neutral pH range for the entire simulation period. Therefore, the lack of available data for these parameters does not limit model application. Conversely, k_{H^+} and k_W have a significant impact on the model response. A five-fold decrease of k_{H^+} and k_W (case 2.2) increased $t_{99\%}$ to 52.3 d (twice as long as the base case). When these two parameters were an order of magnitude smaller than in the base case (case 2.3), 99% degradation of PCE was not achieved. Hence, k_{H^+} and k_W directly control the mineral dissolution rate: When they are too low compared with the CAH degradation rate, the pH drops rapidly inhibiting bacterial activity. Similarly, the security factor D has a significant impact on the model output (case 6). An increase of D from 15 to 50 increased $t_{99\%}$ by 29.6 d.

3.4.2 Influence of activation energy

The influence of the activation energy terms E_{H^+} and E_W on the model response is very limited. E_{H^+} was varied between 18.9 to 132 kJ mol^{-1} and E_W between 51 and 104 .9 kJ mol^{-1}, corresponding to the minimum and maximum values observed for the 20 selected minerals (case 5). The resulting $\Delta t_{99\%}$ was equal to -0.2 d (minimal values of the activation energy) and 2.7 d (maximal values of activation energy). Activation energy controls the changes in the mineral dissolution rate when temperature is different from 25°C. The simulations reported here considered a temperature of 20°C fairly close to the reference value, which partially explains the weak sensitivity. Further numerical simulations with lower temperatures (e.g., 10°C) indicated that, for typical groundwater temperatures, the influence of activation energies remains limited.

3.4.3 Influence of solubility constant

Riebeckite has the smallest solubility constant among the minerals considered (log K_D = -7.87). For this value (case 7.1), the target 99% PCE degradation is not reached as the solution rapidly equilibrates with the mineral phase and dissolution halts. Only a total of 0.16 mmol of mineral dissolved within 25 d (compared to 7 mmol l^{-1} for the base case). Conversely, an increase of the solubility constant up to 68.4 (value for chlorite) reduced $t_{99\%}$ to its minimum value, i.e., 17 d (case 7.2), which corresponds to an optimal pH over the entire simulation period. In this case, the solution always remained far from equilibrium with the mineral phase and mineral dissolution was only controlled by kinetics.

3.4.4 Influence of temperature

A 10°C decrease in temperature increased $t_{99\%}$ to 62.9 d (2.5 fold increase) (case 9.1). In the simulations, temperature changes affect the mineral dissolution rates and solubility constants.

The influence of temperature on the dechlorination rate was instead not taken into account and the same parameters for biological transformations estimated at 20°C were used. The reason for this approximation was the lack of information about the extent of reduction of the dechlorination rate with temperature for the PM consortium. Zhuang and Pavlostathis (1995) studied the influence of temperature on a ORB mixed culture and showed that the rate was approximately halved reducing the temperature from 20 to 15°C. On the other hand, a change in ambient temperature from 20 to 15°C leads to a decrease of the mineral dissolution rate of fayalite by a factor of 1.8 (Eq. 15). This suggests that, in the temperature range 10-20°C, the change in dechlorination rate will be similar to the change in dissolution rate and buffering capacity of the mineral, with little or no effect on the ability of the mineral to counterbalance the acidity produced. The $t_{99\%}$ value will increase nevertheless, as the rate at which CAHs are transformed is reduced at lower temperatures.

3.4.5 Cation inhibition function

The goal of case 10 was to evaluate the importance of the base cations inhibition terms f_{H^+} and f_W in Eq. 15. As discussed previously, these parameters are available for few minerals only and it was therefore important to ascertain the resulting error on model predictions. For the groundwater composition considered in this simulations, the decrease in dechlorination efficiency when the inhibition terms are considered is relatively small, $\Delta t_{99\%}$ = 4.4 d. This value should be compared with that resulting from the uncertainty in the kinetic rate parameters k_{H^+} and k_W, which is five or more times larger ($\Delta t_{99\%}$ > 20 d). As a result, the two inhibition terms can be neglected for the conditions used. For higher concentrations of Al^{3+}, Na^+, K^+ and Mg^{2+}, this choice should be tested further. For example, additional calculations showed that, for the case where the sum of the activities of the base cations exceeds 20 mmol l^{-1}, the dissolution rate of K-feldspar is halved.

3.4.6 Surface area evolution

Case 11 investigated the effect of changing the parameter α in Eq. 18, that is, the equation governing the change in reactive surface area as mineral dissolution proceeds. The parameter was changed from 0.67 – which corresponds to a monodisperse population of spherical grains – to 3.4, the value for a lognormal grain size distribution. Simulation results showed a $\Delta t_{99\%}$ = 1.9 d. It was then concluded that this parameter has little influence, and uncertainties in its determination introduce only a small change in simulation results.

3.4.7 Summary of global sensitivity analyses

Results of global sensitivity analyses demonstrated that the most influent parameters are the solubility constant, K_D, and the kinetic dissolution rate constants in the acidic and neutral range k_H^+ and k_W. The security factor D also influenced significantly the model response. Experimental determination of the kinetic rate constants is associated with a high level of uncertainty as discussed before. Therefore, additional efforts should be spent to characterize better those parameters, in particular in field conditions. With current knowledge this method can still be successful but it might be necessary to overestimate the amount of mineral to be injected, to guarantee sufficient buffering capacity.

3.5 Comparison among minerals

Additional simulations were used to rank the 12 minerals previously selected on the basis of their solubility in the acid/alkaline pH range (i.e., those belonging to class 3 in Table 6). The minerals were ordered considering the time required to reach 99% degradation of the initial PCE mass, i.e., the more suitable minerals had lower $t_{99\%}$ values. Results are reported in Table 7. Of the twelve minerals tested, five (anorthite, chlorite, diopside, tremolite and enstatite) had a dissolution rate that was too low to counterbalance acidity produced by the

dechlorination. As a result, the target 99% PCE degradation was not reached and byproducts (mainly vinyl chloride) accumulated. Thus, these minerals were excluded from the list of candidate buffers. The kinetic constants k_{H^+} and k_W for these minerals were less than 10^{-8} mol m^2 s^{-1} and 10^{-11} mol m^2 s^{-1}, respectively. Among the remaining eight minerals, $t_{99\%}$ varied from 21 d (nepheline) to 54 d (andradite). The minerals with smaller $t_{99\%}$ (< 30 d), namely nepheline, fayalite, glaucophane and lizardite, are the best candidates as acid-neutralizing agents. This result is partially corroborated by Kleiv and Sandvik (2000), who recognized the buffering properties of nepheline. The amount of mineral consumed to buffer the same amount of PCE was also computed (Table 7). Only relatively small variations were found, ranging from 0.32 to 0.97 g mineral consumed per mmol of PCE transformed. According to simulation results, dechlorination of 1.5 mmol of PCE will consume 0.7 to 1.5 g l^{-1} of mineral for a period of approximately one month, depending on the mineral used.

4 Summary and conclusions

The importance of groundwater pH control for enhanced *in situ* bioremediation of CAHs as well as other remediation technologies is well recognized. A batch biogeochemical model was implemented to evaluate the use of silicate minerals as buffering agents during the treatment of contaminated sites. To the best of our knowledge, this is the first study focusing on the use of silicate mineral powder in aquifers. Although in this work the technology was applied to the specific case of CAH bioremediation, the geochemical model could be applied to other remediation processes requiring maintenance of neutral pH. As it stands, the model can be used as a design tool to calculate the amount of mineral needed. This requires the knowledge of the initial mass of CAHs.

Eight potentially suitable minerals were identified through the screening methodology. The other silicate minerals were excluded as their dissolution kinetic was too low to neutralize

the acidity produced by the biological processes. The most promising candidate was nepheline, due to its relatively rapid dissolution rate. This result extends the work of Kleiv and Sandvik (2000), who proposed its use as buffering agent for heavy metal stabilization. The minerals considered in this study can be easily found on the market, as they are used in industrial processes (such as glass making, ceramics, abrasive) or in mine tailings, and are therefore relatively inexpensive. In the context of field application, the local availability of the mineral should also be assessed. The minerals considered in this study are distributed worldwide and mineralogical databases (e.g., www.mindat.org) can be used to identify local deposits and availability. For this reason, a detailed evaluation of the treatment costs, although important, is site-specific and was beyond the scope of this study.

A sensitivity analyses was conducted to identify the parameters that control the model response and therefore need accurate characterization. It was observed that the most influential parameters are the mineral dissolution rates in the acidic and neutral ranges, k_{H^+} and k_W, the reaction order for protons promoted dissolution, n_{H^+}, and the solubility constant K_D. Due to the large uncertainties associated with the determination of the kinetic rate constants, the results of the sensitivity analysis suggested that model predictions should be further verified. Groundwater temperature is also important, as it controls both the rate of acidity production and the buffering capacity of the mineral.

The model includes the main geochemical and microbial processes that control pH evolution. Interactions between minerals and microorganisms were, however, neglected due to the lack of reliable data. Possible feedbacks include the microbial enhancement of mineral weathering rates (Barker et al. 1998; Ullman et al. 1996; Vandevivere et al. 1994) and the inhibition of bacteria by trace elements release during mineral dissolution (Dopson et al. 2008). The other important process not included in the model is the possible passivation of

the mineral reactive surface due to secondary phase precipitation, which would decrease the dissolution rate and buffering capacity. Microcosm experiments are currently being conducted to validate the model and ascertain the importance of the different modeling assumptions.

Acknowledgements

This work was funded by the Swiss National Science Foundation (SNSF) (200021-120160/1). The authors thank Nicolas Meisser (Cantonal Geology Museum, UNIL, Lausanne) for his useful insights on the theory of mineral dissolution, and the reviewers for their insightful comments.

References

Aagaard, P., & Helgeson, H. C. (1982). Thermodynamic and kinetic constraints on reaction-rates among minerals and aqueous-solutions.1. Theoretical considerations. *American Journal of Science, 282*(3), 237-285, doi:10.2475/ajs.282.3.237.

Adamson, D. T., Lyon, D. Y., & Hughes, J. B. (2004). Flux and product distribution during biological treatment of tetrachloroethene dense non-aqueous-phase liquid. *Environmental Science & Technology, 38*(7), 2021-2028, doi:10.1021/es034737a.

AFCEE (2004).Principles and Practices of Enhanced Anaerobic Bioremediation of Chlorinated Solvents. Washington, DC: US Department of defense, Air Force Center for Environmental Excellence and the Environmental Security Technology Certification Program (ESTCP).

Alkattan, M., Oelkers, E. H., Dandurand, J. L., & Schott, J. (1998). An experimental study of calcite and limestone dissolution rates as a function of pH from -1 to 3 and temperature from 25 to 80 degrees C. *Chemical Geology, 151*(1-4), 199-214, doi:10.1016/s0009-2541(98)00080-1.

Allison, J. D., Brown, D. S., & Novo-Gradac, K. J. (1991).MINTEQA2/PRODEF2 - A Geochemical Assessment Model for Environmental Systems: Version 4.0. User's Manual. Environmental Research Laboratory, Office of Research and Development, U.S. Environmental Protection Agency, Athens, Georgia.

Amos, B. K., Suchomel, E. J., Pennell, K. D., & Loffler, F. E. (2008). Microbial activity and distribution during enhanced contaminant dissolution from a NAPL source zone. *Water Research, 42*(12), 2963-2974, doi:10.1016/j.watres.2008.03.015.

Appelo, C. A. J., & Postma, D. (2005). *Geochemistry, Groundwater and Pollution*. Leiden, The Netherlands: AA Balkema Publishers.

Aulenta, F., Majone, M., & Tandoi, V. (2006). Enhanced anaerobic bioremediation of chlorinated solvents: environmental factors influencing microbial activity and their relevance under field conditions. *Journal of Chemical Technology and Biotechnology, 81*(9), 1463-1474, doi:10.1002/jctb.1567.

Aulenta, F., Pera, A., Rossetti, S., Papini, M. P., & Majone, M. (2007). Relevance of side reactions in anaerobic reductive dechlorination microcosms amended with different electron donors. *Water Research, 41*(1), 27-38, doi:10.1016/j.watres.2006.09.019.

Bailey, J. E., & Ollis, D. F. (1986). *Biochemical engineering fundamentals. 2nd edition.* New-York: McGraw-Hill.

Barker, W. W., Welch, S. A., Chu, S., & Banfield, J. F. (1998). Experimental observations of the effects of bacteria on aluminosilicate weathering. *American Mineralogist, 83*(11-12), 1551-1563.

Berg, A., & Banwart, S. A. (2000). Carbon dioxide mediated dissolution of Ca-feldspar: implications for silicate weathering. *Chemical Geology, 163*(1-4), 25-42, doi:10.1016/s0009-2541(99)00132-1.

Blanc, P., Lassin, A., & Piantone, P. (2007).Thermoddem a database devoted to waste minerals. BRGM, Orléans, France. http://thermoddem.brgm.fr.

Borkovec, M., Wu, Q., Degovics, G., Laggner, P., & Sticher, H. (1993). Surface-area and size distributions of soil particles. *Colloids and Surfaces A: Physicochemical and Engineering Aspects, 73*, 65-76, doi:10.1016/0927-7757(93)80007-2.

Brandt, F., Bosbach, D., Krawczyk-Barsch, E., Arnold, T., & Bernhard, G. (2003). Chlorite dissolution in the acid pH-range: A combined microscopic and macroscopic approach. *Geochimica et Cosmochimica Acta, 67*(8), 1451-1461, doi:10.1016/s0016-7037(02)01293-0.

Brantley, S. L., Kubicki, J. D., & White, A. F. (2008). *Kinetics of water-rock interaction*. New York: Springer.

Chou, L., & Wollast, R. (1984). Study of the weathering of albite at room-temperature and pressure with a fluidized-bed reactor. *Geochimica et Cosmochimica Acta, 48*(11), 2205-2217, doi:10.1016/0016-7037(84)90217-5.

Chu, M., Kitanidis, P. K., & McCarty, P. L. (2004). Possible factors controlling the effectiveness of bioenhanced dissolution of non-aqueous phase tetrachloroethene. *Advances in Water Resources, 27*(6), 601-615, doi:10.1016/j.advwatres.2004.03.002.

Cope, N., & Hughes, J. B. a. (2001). Biologically-enhanced removal of PCE from NAPL source zones. *Environmental Science & Technology, 35*(10), 2014-2021.

Cupples, A. M., Spormann, A. M., & McCarty, P. L. (2004). Comparative evaluation of chloroethene dechlorination to ethene by *Dehalococcoides*-like microorganisms. *Environmental Science & Technology, 38*(18), 4768-4774, doi:10.1021/es049965z.

Curtis, G. P. (2003). Comparison of approaches for simulating reactive solute transport involving organic degradation reactions by multiple terminal electron acceptors. *Computers & Geosciences, 29*(3), 319-329, doi:10.1016/s0098-3004(03)00008-6.

Czupyrna, G. (1989). *In situ immobilization of heavy-metal-contaminated soils*. Noyes Data Corp.

Davis, J. A., & Hayes, K. F. Geochemical processes at mineral surfaces. In S. American Chemical (Ed.), *American Chemical Society, Meeting, Washington D.C, USA*, 1986.

Dixon, D. G., & Hendrix, J. L. (1993). Theoretical basis for variable order assumption in the kinetics of leaching of discrete grains. *Aiche Journal, 39*(5), 904-907, doi:10.1002/aic.690390520.

Dopson, M., Halinen, A. K., Rahrmen, N., Bostrom, D., Sundkvist, J. E., Riekkola-Vanhanen, M., et al. (2008). Silicate mineral dissolution during heap bioleaching. *Biotechnology and Bioengineering, 99*(4), 811-820, doi:10.1002/bit.21628.

Emmanuel, S., & Berkowitz, B. (2005). Mixing-induced precipitation and porosity evolution in porous media. *Advances in Water Resources, 28*(4), 337-344, doi:10.1016/j.advwatres.2004.11.010.

Fennell, D. E., & Gossett, J. M. (1998). Modeling the production of and competition for hydrogen in a dechlorinating culture. *Environmental Science & Technology, 32*(16), 2450-2460, doi:10.1021/es980136l.

Fernandez-Caliani, J. C., Barba-Brioso, C., & Perez-Lopez, R. (2008). Long-term interaction of wollastonite with acid mine water and effects on arsenic and metal removal. *Applied Geochemistry, 23*(5), 1288-1298, doi:10.1016/j.apgeochem.2007.11.018.

Fetzner, S. (1998). Bacterial dehalogenation. *Applied Microbiology and Biotechnology, 50*(6), 633-657, doi:10.1007/s002530051346.

Gaus, I., Audigane, P., Andre, L., Lions, J., Jacquemet, N., Dutst, P., et al. (2008). Geochemical and solute transport modeling for CO2 storage, what to expect from it? *International Journal of Greenhouse Gas Control, 2*(4), 605-625, doi:10.1016/j.ijggc.2008.02.011.

Gautier, J. M., Oelkers, E. H., & Schott, J. (2001). Are quartz dissolution rates proportional to BET surface areas? *Geochimica et Cosmochimica Acta, 65*(7), 1059-1070, doi:10.1016/s0016-7037(00)00570-6.

Golubev, S. V., Pokrovsky, O. S., & Schott, J. (2005). Experimental determination of the effect of dissolved CO2 on the dissolution kinetics of Mg and Ca silicates at 25 degrees C. *Chemical Geology, 217*(3-4), 227-238, doi:10.1016/j.chemgeo.2004.12.011.

Hamilton, J. P., Brantley, S. L., Pantano, C. G., Criscenti, L. J., & Kubicki, J. D. (2001). Dissolution of nepheline, jadeite and albite glasses: Toward better models for aluminosilicate dissolution. *Geochimica et Cosmochimica Acta, 65*(21), 3683-3702, doi:10.1016/S0016-7037(01)00724-4.

Helgeson, H. C., Murphy, W. M., & Aagaard, P. (1984). Thermodynamic and kinetic constraints on reaction-rates among minerals and aqueous-solution.2. Rate constants, effective surface-area, and the hydrolysis of feldspar. *Geochimica et Cosmochimica Acta, 48*(12), 2405-2432.

Hodson, M. E. (2006). Does reactive surface area depend on grain size? Results from pH 3, 25°C far-from-equilibrium flow-through dissolution experiments on anorthite and biotite. *Geochimica et Cosmochimica Acta, 70*(7), 1655-1667, doi:10.1016/j.gca.2006.01.001.

Holliger, C., Schraa, G., Stams, A. J. M., & Zehnder, A. J. B. (1993). A highly purified enrichment culture couples the reductive dechlorination of tetrachloroethene to growth. *Applied and Environmental Microbiology, 59*(9), 2991-2997.

ITRC (2005).Technical and Regulatory Guidance for In Situ Chemical Oxidation of Contaminated Soil and Groundwater, 2nd ed. ISCO-2

Kieffer, B., Jove, C. F., Oelkers, E. H., & Schott, J. (1999). An experimental study of the reactive surface area of the Fontainebleau sandstone as a function of porosity, permeability, and fluid flow rate. *Geochimica et Cosmochimica Acta, 63*(21), 3525-3534, doi:10.1016/s0016-7037(99)00191-x.

Kleiv, R. A., & Sandvik, K. L. (2000). Using tailings as heavy metal adsorbents - The effect of buffering capacity. *Minerals Engineering, 13*(7), 719-728.

Knauss, K. G., Nguyen, S. N., & Weed, H. C. (1993). Diopside dissolution kinetics as a function of pH, CO2, temperature and time. *Geochimica et Cosmochimica Acta, 57*(2), 285-294.

Knauss, K. G., & Wolery, T. J. (1986). Dependence of albite dissolution kinetics on pH and time at 25-degrees-C and 70 degrees-C. *Geochimica et Cosmochimica Acta, 50*(11), 2481-2497, doi:10.1016/0016-7037(86)90031-1.

Kouznetsova, I., Mao, X. M., Robinson, C., Barry, D. A., Gerhard, J. I., & McCarty, P. L. (2010). Biological reduction of chlorinated solvents: Batch-scale geochemical modeling. *Advances in Water Resources, 33*(9), 969-986, doi:10.1016/j.advwatres.2010.04.017.

Krumholz, L. R. (1997). *Desulfuromonas chloroethenica* sp. nov. uses tetrachloroethylene and trichloroethylene as electron acceptors. *International Journal of Systematic Bacteriology, 47*(4), 1262-1263.

Lasaga, A. C. (1995). Fundamentals approaches in describing mineral dissolution and precipitation rates. In A. F. White, & S. L. Brantley (Eds.), *Chemical Weathering Rate of Silicate Minerals, Reviews in Mineralogy*. (pp. 23-86). Mineralogic Society of America.

Lee, Y. J., Miyahara, T., & Noike, T. (2002). Effect of pH on microbial hydrogen fermentation. *Journal of Chemical Technology and Biotechnology, 77*(6), 694-698, doi:10.1002/jctb.623.

Lichtner, P. C. (1988). The quasi-stationary state approximation to coupled mass-transport and fluid-rock interaction in a porous-medium. *Geochimica et Cosmochimica Acta, 52*(1), 143-165, doi:10.1016/0016-7037(88)90063-4.

Likens, G. E., Buso, D. C., Dresser, B. K., Bernhardt, E. S., Hall, R. O., Macneale, K. H., et al. (2004). Buffering an acidic stream in New Hampshire with a silicate mineral. *Restoration Ecology, 12*(3), 419-428.

Loffler, F. E., Tiedje, J. M., & Sanford, R. A. (1999). Fraction of electrons consumed in electron acceptor reduction and hydrogen thresholds as indicators of halorespiratory physiology. *Applied and Environmental Microbiology, 65*(9), 4049-4056.

Lowson, R. T., Comarmond, M. C. J., Rajaratnam, G., & Brown, P. L. (2005). The kinetics of the dissolution of chlorite as a function of pH and at 25 degrees C. *Geochimica et Cosmochimica Acta, 69*(7), 1687-1699, doi:10.1016/j.gca.2004.09.028.

Lozecznik, S., Sparling, R., Oleszkiewicz, J. A., Clark, S., & VanGulck, J. F. (2010). Leachate treatment before injection into a bioreactor landfill: Clogging potential reduction and benefits of using methanogenesis. *Waste Management, 30*(11), 2030-2036, doi:10.1016/j.wasman.2010.04.024.

Marini, L. (2007). *Geological sequestration of carbon dioxide: thermodynamics, kinetics, and reaction path modeling*. Elsevier.

Mast, M. A., & Drever, J. I. (1987). The effect of oxalate on the dissolution rates of oligoclase and tremolite. *Geochimica et Cosmochimica Acta, 51*(9), 2559-2568.

MaymoGatell, X., Chien, Y. T., Gossett, J. M., & Zinder, S. H. (1997). Isolation of a bacterium that reductively dechlorinates tetrachloroethene to ethene. *Science, 276*(5318), 1568-1571, doi:10.1126/science.276.5318.1568.

McCarty, P. L., Chu, M. Y., & Kitanidis, P. K. a. (2007). Electron donor and pH relationships for biologically enhanced dissolution of chlorinated solvent DNAPL in groundwater. *European Journal of Soil Biology, 43*(5-6), 276-282, doi:10.1016/j.ejsobi.2007.03.004.

Metz, V., & Ganor, J. (2001). Stirring effect on kaolinite dissolution rate. *Geochimica et Cosmochimica Acta, 65*(20), 3475-3490.

Mussati, M. C., Fuentes, M., Aguirre, P. A., & Scenna, N. J. (2005). A steady-state module for modeling anaerobic biofilm reactors. *Latin American Applied Research, 35*(4), 255-263.

Neumann, A., Scholzmuramatsu, H., & Diekert, G. (1994). Tetrachloroethene metabolism of *Dehalospirillum multivorans*. *Archives of Microbiology, 162*(4), 295-301.

Oelkers, E. H., & Schott, J. (2001). An experimental study of enstatite dissolution rates as a function of pH, temperature, and aqueous Mg and Si concentration, and the mechanism of pyroxene/pyroxenoid dissolution. *Geochimica et Cosmochimica Acta, 65*(8), 1219-1231, doi:10.1016/s0016-7037(00)00564-0.

Palandri, J. L., & Kharaka, Y. K. (2004).A compilation of rate parameters of water-mineral interaction kinetics for application to geochemical modeling. U.S. Geological Survey Open File Report 2004-1068.

Parkhurst, D. L., & Appelo, C. A. J. (1999).User's Guide to PHREEQC—a computer program for speciation, reaction-path, 1D-transport, and inverse geochemical calculations. Technical Report 99-4259. Water-Resources Investigations. Report 99-4259. Denver, CO: U.S. Geological Survey.

Payne, F. C., Suthersan, S. S., Nelson, D. K., Suarez, G., Tasker, I., & Akladiss, N. (2006). Enhanced reductive dechlorination of PCE in unconsolidated soils. *Remediation Journal, 17*(1), 5-21, doi:10.1002/rem.20109.

Pokrovsky, O. S., & Schott, J. (2000). Kinetics and mechanism of forsterite dissolution at 25 degrees C and pH from 1 to 12. *Geochimica et Cosmochimica Acta, 64*(19), 3313-3325.

Robinson, C., & Barry, D. A. (2009). Design tool for estimation of buffer requirement for enhanced reductive dechlorination of chlorinated solvents in groundwater. *Environmental Modelling and Software, 24*(11), 1332-1338, doi:10.1016/j.envsoft.2009.03.012.

Robinson, C., Barry, D. A., McCarty, P. L., Gerhard, J. I., & Kouznetsova, I. (2009). pH control for enhanced reductive bioremediation of chlorinated solvent source zones. *Science of the Total Environment, 407*(16), 4560-4573, doi:10.1016/j.scitotenv.2009.03.029.

Roychowdhury, S., Cox, D., & Levandowsky, M. (1988). production of hydrogen by microbial fermentation. *International Journal of Hydrogen Energy, 13*(7), 407-410.

Schepers, A. W., Thibault, J., & Lacroix, C. (2002). *Lactobacillus helveticus* growth and lactic acid production during pH-controlled batch cultures in whey permeate/yeast extract medium. Part II: kinetic modeling and model validation. *Enzyme and Microbial Technology, 30*(2), 187-194.

Scholz-Muramatsu, H., Neumann, A., Messmer, M., Moore, E., & Diekert, G. (1995). Isolation and characterization of *Dehalospirillum multivorans* gen. nov., sp. nov., a tetrachloroethene-utilizing, strictly anaerobic bacterium. *Archives of Microbiology, 163*(1), 48-56.

Schott, J., & Berner, R. A. (1985). Dissolution mechanisms of pyroxenes and olivines during weathering. In J. I. Drever (Ed.), *The Chemistry of Weathering* Hingham, Massachusetts, USA: Kluwer Academic.

Scislewski, A., & Zuddas, P. (2010). Estimation of reactive mineral surface area during water-rock interaction using fluid chemical data. *Geochimica et Cosmochimica Acta, 74*(24), 6996-7007, doi:10.1016/j.gca.2010.09.015.

Sung, Y., Ritalahti, K. M., Sanford, R. A., Urbance, J. W., Flynn, S. J., Tiedje, J. M., et al. (2003). Characterization of two tetrachloroethene-reducing, acetate-oxidizing anaerobic bacteria and their description as *Desulfuromonas michiganensis* sp. nov. *Applied and Environmental Microbiology, 69*(5), 2964-2974.

Suyama, A., Iwakiri, R., Kai, K., Tokunaga, T., Sera, N., & Furukawa, K. (2001). Isolation and characterization of *Desulfitobacterium* sp strain Y51 capable of efficient dehalogenation of tetrachloroethene and polychloroethanes. *Bioscience Biotechnology and Biochemistry, 65*(7), 1474-1481.

Sverdrup, H. (1990). *The kinetics of base cation release due to chemical weathering*. University Press, Lund, Sweden.

Sverdrup, H. U., & Warfvinge, P. (1995). Estimating field weathering rates using laboratory kinetics of primary silicate minerals in natural soil environment in relation to a chemical weathering model. In A. F. White, & S. L. Brantley (Eds.), *Chemical weathering rates of silicates of silicate minerals*. (Vol. Rev. Mineral.31, pp. 485-541).

Tole, M. P., Lasaga, A. C., Pantano, C., & White, W. B. (1986). The kinetics of dissolution of nepheline (NaAlSiO4). *Geochimica et Cosmochimica Acta, 50*(3), 379-392.

Ullman, W. J., Kirchman, D. L., Welch, S. A., & Vandevivere, P. (1996). Laboratory evidence for microbially mediated silicate mineral dissolution in nature. *Chemical Geology, 132*(1-4), 11-17.

Vainberg, S., Condee, C. W., & Steffan, R. J. (2009). Large-scale production of bacterial consortia for remediation of chlorinated solvent-contaminated groundwater. *Journal of Industrial Microbiology & Biotechnology, 36*(9), 1189-1197, doi:10.1007/s10295-009-0600-5.

Vandevivere, P., Welch, S. A., Ullman, W. J., & Kirchman, D. L. (1994). Enhanced dissolution of silicate minerals by bacteria at near-neutral pH. *Microbial Ecology, 27*(3), 241-251.

Vangrinsven, J. J. M., & Vanriemsdijk, W. H. (1992). Evaluation of batch and column techniques to measure weathering rates in soils. *Geoderma, 52*(1-2), 41-57.

Weissbart, E. J., & Rimstidt, J. D. (2000). Wollastonite: Incongruent dissolution and leached layer formation. *Geochimica et Cosmochimica Acta, 64*(23), 4007-4016.

White, A. F., Blum, A. E., Schulz, M. S., Bullen, T. D., Harden, J. W., & Peterson, M. L. (1996). Chemical weathering rates of a soil chronosequence on granitic alluvium .1. Quantification of mineralogical and surface area changes and calculation of primary silicate reaction rates. *Geochimica et Cosmochimica Acta, 60*(14), 2533-2550.

White, A. F., & Brantley, S. L. (1995). *Chemical weathering rates of silicate minerals*. Mineralogical Society of America.

White, A. F., & Brantley, S. L. (2003). The effect of time on the weathering of silicate minerals: why do weathering rates differ in the laboratory and field? *Chemical Geology, 202*(3-4), 479-506, doi:10.1016/j.chemgeo.2003.03.001.

Witkamp, G. J., Vandereerden, J. P., & Vanrosmalen, G. M. (1990). Growth of Gypsum. 1. Kinetics. *Journal of Crystal Growth, 102*(1-2), 281-289, doi:10.1016/0022-0248(90)90912-5.

Wogelius, R. A., & Walther, J. V. (1992). Olivine dissolution kinetics at near-surface conditions. *Chemical Geology, 97*(1-2), 101-112.

Yang, Y. R., & McCarty, P. L. (2000). Biologically enhanced dissolution of tetrachloroethene DNAPL. *Environmental Science & Technology, 34*(14), 2979-2984.

Yang, Y. R., & McCarty, P. L. (2002). Comparison between donor substrates for biologically enhanced tetrachloroethene DNAPL dissolution. *Environmental Science & Technology, 36*(15), 3400-3404, doi:10.1021/es011408e.

Yaws, C. L. (1999). *Chemical properties handbook: physical, thermodynamic, environmental, transport, safety, and health related properties for organic and inorganic chemicals*. New York, USA: McGraw-Hill.

Yu, S., & Semprini, L. (2004). Kinetics and modeling of reductive dechlorination at high PCE and TCE concentrations. *Biotechnology and Bioengineering, 88*(4), 451-464.

Zhang, H., & Bloom, P. R. (1999). The pH dependence of hornblende dissolution. *Soil Science, 164*(9), 624-632.

Zhu, C., Lu, P., Zheng, Z. P., & Ganor, J. (2010). Coupled alkali feldspar dissolution and secondary mineral precipitation in batch systems: 4. Numerical modeling of kinetic reaction paths. *Geochimica et Cosmochimica Acta, 74*(14), 3963-3983, doi:10.1016/j.gca.2010.04.012.

Zhuang, P., & Pavlostathis, S. G. (1995). Effect of temperature, pH and electron-donor on the microbial reductive dechlorination of chloroalkenes. *Chemosphere, 31*(6), 3537-3548, doi:10.1016/0045-6535(95)00204-L.

Tables

Table 1 Dissolution reactions and thermodynamic parameters of the selected silicate minerals.

Silicate mineral	Dissolution reaction	Log K_D (T = 25°C) [a]	ΔH [J mol^{-1}] [a]
Albite	$NaAlSi_3O_8 + 4H^+ + 4H_2O = Al^{3+} + Na^+ + 3H_4SiO_4$	4.14	-95 623
Almandine	$Fe_3Al_2Si_3O_{12} + 12H^+ = 2Al^{3+} + 3Fe^{2+} + 3H_4SiO_4$	42.16	-465 683
Andradite	$Ca_3Fe_2Si_3O_{12} + 10H^+ + H2O = 0.5O_2 + 3Ca^{2+} + 2Fe^{2+} + 3H_4SiO_4$	16.79	-137 101
Anorthite	$Ca(Al_2Si_2)O_8 + 8H^+ = 2Al^{3+} + Ca^{2+} + 2H_4SiO_4$	25.31	-314 358
Chlorite	$Mg_5Al_2Si_3O_{10}(OH)_8 + 16H^+ = 5Mg^{2+} + 2Al^{3+} + 3H_4SiO_4 + 6H2O$	68.38[b]	-634 275[b]
Cordierite	$Mg_2Al_3(AlSi_5)O_{18} + 16H^+ + 2H2O = 4Al^{3+} + 2Mg^{2+} + 5H_4SiO_4$	49.41	-660 411
Diopside	$CaMg(SiO_3)_2 + 4H^+ + 2H_2O = Ca^{2+} + Mg^{2+} + 2H_4SiO_4$	21.73	-158 241
Enstatite	$MgSiO_3 + 2H^+ + 1H_2O = Mg^{2+} + H_4SiO_4$	11.83	-95 552
Fayalite	$Fe_2SiO_4 + 4H^+ = 2Fe^{2+} + H_4SiO_4$	19.02	-159 491
Forsterite	$Mg_2SiO_4 + 4H^+ = 2Mg^{2+} + H_4SiO_4$	28.60	-219 449
Glaucophane	$Na_2(Mg_3Al_2)Si_8O_{22}(OH)_2 + 14H^+ + 8H_2O = 2Al^{3+} + 3Mg^{2+} + 2Na^+ + 8H_4SiO_4$	36.99	-397 394
Grossular	$Ca_3Al_2Si_3O_{12} + 12H^+ = 2Al^{3+} + 3Ca^{2+} + 3H_4SiO_4$	49.36	-449 383
Jadeite	$NaAl(SiO_3)_2 + 4H^+ + 2H_2O = Al^{3+} + Na^+ + 2H_4SiO_4$	7.55	-100 168
Leucite	$KAlSi_2O_6 + 2H_2O + 4H^+ = 2H_4SiO_4 + Al^{3+} + K^+$	6.42 [c]	-92 465[c]
Lizardite	$Mg_3Si_2O_5(OH)_4 + 6H^+ = 3Mg^{2+} + H_2O + 2H_4SiO_4$	32.56	-245 718
Nepheline	$Na(AlSi)O_4 + 4H^+ = Al^{3+} + Na^+ + H_4SiO_4$	14.07	-146 839
Riebeckite	$Na_2(Fe_3Fe_2)Si_8O_{22}(OH)_2 + 12H^+ + 9H_2O = 0.5O_2 + 5Fe^{2+} + 2Na^+ + 8H_4SiO_4$	-7.81	-18 281
Spodumene	$LiAlSi_2O_6 + 4H^+ = + Al^{3+} + Li^+ + 2H_2O + 2SiO_2$	6.99 [d]	-89 181[d]
Tremolite	$(Ca_2Mg_5)Si_8O_{22}(OH)_2 + 14H^+ + 8H_2O = 2Ca^{2+} + 5Mg^{2+} + 8H_4SiO_4$	67.25	-520 914
Wollastonite	$CaSiO_3 + 2H^+ + H_2O = Ca^{2+} + H_4SiO_4$	14.02	-88 220

[a] from THERMODDEM database except where indicated otherwise

[b] from PHREEQC database

[c] from MINTEQ database

[d] from LLNL database

Table 2 Dissolution rate kinetic parameters of selected silicate minerals obtained by fitting Eq. 1 to literature datasets.

Silicate mineral	Acid mechanism		Neutral mechanism	Basic mechanism		Reference of datasets
	$\log k_{H^+}$ log [mol m^{-2} s^{-1}]	n_{H^+}	$\log k_W$ log [mol m^{-2} s^{-1}]	$\log k_{OH^-}$ log [mol m^{-2} s^{-1}]	n_{OH^-}	
Albite	[-11; -10.16]	[0.457; 1]	[-12.4; -12.56]	[-16.3; -15.6]	[-0.5; -0.572]	Chou and Wollast (1984); Knauss and Wolery (1986)
Almandine	-5.2	1	-10.7	-13.71	-0.35	Sverdrup (1990)
andradite	-5.2	1	-10.7	-	-	Sverdrup (1990)
Anorthite	-8.2	0.55	-11.2	-	-	Berg and Banwart (2000); Hodson (2006)
Chlorite	[-10.9;-9.79]	[0.25-0.49]	-13	-16.79	-0.43	Brandt et al. (2003); Lowson (2005)
Cordierite	-3.8	1	-11.2	-	-	Sverdrup (1990)
Diopside	[-8.88; -9.46]	[0.28;0.41]	[-11.21; -11.01]	-	-	Knauss et al. (1993); Golubev et al.(2005)
Enstatite	[-8.98; -9.02]	[0.24; 0.6]	-12.72	-	-	Schott and Berner (1985); Oelkers and Schott (2001)
Fayalite	[-5.9; -4.8]	[0.69; 1]	-9.5	-	-	Sverdrup (1990); Wogelius and Walther (1992)
Forsterite	[-6.78; -6.70]	[0.37; 0.74]	[-10.7; -10.1]	-	-	Pokrovsky and Schott (2000) Golubev et al. (2005)
Glaucophane	-5.6	0.7	-10.1	-	-	Sverdrup (1990)
Grossular	-5.1	1	-10.7	-	-	Sverdrup (1990)
Jadeite	[-8.82; -6]	[0.7; 0.72]	[-12; -9.5]	-14	-0.3	Sverdrup (1990); Hamilton et al. (2001)
Leucite	-6	0.7	-9.2	-	-	Sverdrup (1990)
Lizardite	-5.7	0.8	-12.4	-	-	Sverdrup (1990)
Nepheline	-3.47	0.97	-8.61	-	-	Tole et al. (1986)
Riebeckite	-7.7	0.7	-12.2	-	-	Sverdrup (1990)
Spodumene	-4.6	0.7	-9.3	-	-	Sverdrup (1990)
Tremolite	[-11.9; -8.4]	[0; 0.7]	[-12.5; -10.6]	-	-	Mast and Drever (1987); Sverdrup (1990)
Wollastonite	[-8.72;-7.13]	[0; 0.28]	-	-	-	Weissbart and Rimstidt (2000); Golubev et al (2005)

Table 3 Activation energy terms of silicate mineral dissolution in acid, neutral and basic range [a].

Silicate mineral	Activation energy		
	E_{H^+} [kJ mol^{-1}]	E_W [kJ mol^{-1}]	E_{OH^-} [kJ mol^{-1}]
Albite	65	69.8	71
Almandine	94.4	103.8	37.8
Andradite	94.41	103.8	n.d.[b]
Anorthite	16.6	17.8	n.d.
Chlorite	88	88	88
Cordierite	113.3	28.3	n.d.
Diopside	96.1	40.6	n.d.
Enstatite	80	80	n.d.
Fayalite	94.4	94.4	n.d.
Forsterite	67.2	79	n.d.
Glaucophane	85	94.4	n.d.
Grossular	85	103.8	n.d.
Jadeite	132.2	94.4	n.d.
Leucite	132.2	75.5	56.6
Lizardite	75.5	56.6	n.d.
Nepheline	62.9	65.4	37.8
Riebeckite	56.6	47.2	n.d.
Spodumene	94.4	66.1	n.d.
Tremolite	18.9	94.4	n.d.
Wollastonite	54.7	54.7	n.d.

[a] Data are from Palandri and Kharaka (2004).

[b] n.d. = not determined

Table 4 Parameters for the microbial dechlorination model.

Parameter and units	Value
Maximum degradation rates [μmol mg-protein^{-1} d^{-1}] [a]	
$k_{PCE,max}$	13.3
$k_{TCE,max}$	124
$k_{DCE,max}$	22
$k_{VC,max}$	2.4
Half velocity constants [μmol l^{-1}] [a]	
$K_{s,PCE}$	3.9
$K_{s,TCE}$	2.8
$K_{s,DCE}$	1.9
$K_{s,VC}$	602
Haldane inhibition constants [μmol l^{-1}] [a]	
$K_{H,PCE}$	900
$K_{H,DCE}$	6000
$K_{H,VC}$	7000
Competitive inhibition constants [μmol l^{-1}] [a]	
$K_{CI,PCE}$	3.86
$K_{CI,TCE}$	2.76
$K_{CI,DCE}$	1.90
$K_{CI,VC}$	602.00
Biomass yields [mg-protein/μmol Cl$^-$] [b]	
Y	4.8×10^{-3}
First-order decay constant [d^{-1}] [c]	
k_d	2×10^{-2}
pH inhibition function parameters [d]	
n [-]	3.5
σ [pH units]	2.1
pH_{opt} [pH units]	6.7
Fraction of H_2 used for organohalide respiration [-] [f]	
f_{min}	0.35

[a] Yu and Semprini (2004)
[b] MaymoGatell et al.(1997)
[c] Fennell and Gossett (1998)
[d] Parameters fitted from data of Zhuang and Pavlostathis (1995)
[e] Assumed. The minimal value was chosen as it represents the worst case in term of groundwater acidification.
[f] Average value between 0.2 and 0.5 (AFCEE 2004)
[g] Calculated from (Vangrinsven and Vanriemsdijk 1992)

Table 5 Result of global sensitivity analysis. Case-specific parameters/conditions used and value of $t_{s99\%}$ and $\Delta t_{99\%}$.

Case	Parameters	Units	Base case value	Sensitivity value		
1			BC value	Case 1.1	Case 1.2	
	log k_{OH^-}	log [mol m^{-2} s^{-1}]	-	-16.3	-13.7	
	Results					
	$t_{s99\%}$			25	25	
	$\Delta t_{99\%}$			0	0	
2			BC value	Case 2.1	Case 2.2	Case 2.3
	log k_W	log [mol m^{-2} s^{-1}]	-5.35	-4.85	-5.85	-6.35
	log k_{H^+}	log [mol m^{-2} s^{-1}]	-9.5	-9	-10	-10.5
	Results					
	$t_{s99\%}$			17	52.3	Not reached
	$\Delta t_{99\%}$			-8	27.3	-
3			BC value	Case 3.1	Case 3.2	
	n_{H^+}	-	0.85	0.28	1	
	Results					
	$t_{s99\%}$			17	30.6	
	$\Delta t_{99\%}$			-8	5.6	
4			BC value	Case 4.1	Case 4.2	
	n_{OH^-}	-	0.85	0	1	
	Results					
	$t_{s99\%}$			25	25	
	$\Delta t_{99\%}$			0	0	
5			BC value	Case 5.1	Case 5.2	
	E_W	[kJ mol^{-1}]	94.4	51	104	
	E_{H^+}	[kJ mol^{-1}]	94.4	18.9	132	
	Results					
	$t_{s99\%}$			24.8	27.7	
	$\Delta t_{99\%}$			-0.2	2.7	
6			BC value	Case 6.1	Case 6.2	
	Security factor D	-	15	1	50	
	Results					
	$t_{s99\%}$			17	54.6	
	$\Delta t_{99\%}$			-8	29.6	
7			BC value	Case 7.1	Case 7.2	Case 7.3
	Solubility constant K_D	-	19.02	-7.8	68.4	1
	Results					

	$t_{s99\%}$			not reached	17	43
	$\Delta t_{99\%}$			-	-8	18
8			BC value	Case 8.1		Case 8.2
	Standard enthalpy ΔH	[J mol^{-1}]	159 491	88 220		1 965 817
	Results					
	$t_{s99\%}$			25		25
	$\Delta t_{99\%}$			0		0
9			BC value	Case 9.1		Case 9.2
	Temperature	[°C]	20	10		15
	Results					
	$t_{s99\%}$			62.9		36.4
	$\Delta t_{99\%}$			37.9		11.4
10			BC conditions	Case 10.1		
	Ionic species inhibition f_{H^+}/f_W		f_{H+} =1 ; f_W =1			
	lim BC	-		200		
	xBC			0.3		
	Results					
	$t_{s99\%}$			29		
	$\Delta t_{99\%}$			4		
11			BC conditions	Case 11.1		
	Surface area evolution α	-	0.67	3.4		
	Results					
	$t_{s99\%}$			26.9		
	$\Delta t_{99\%}$			1.9		

Table 6 Mineral classification based on the solubility constant in acid and alkaline conditions. Minerals belonging to class 1 have a solubility at pH 8 in excess of 10 mmol l^{-1}, while minerals belonging to class 2 have a solubility at pH 5 below 1 mmol l^{-1}. Minerals from the third class have a suitable solubility to be used as buffering agent (solubility above 1 mmol l^{-1} at pH 5 and below 10 mmol l^{-1} at pH 8).

Class 1 Excessive solubility at pH 8	Class 2 Insufficient solubility at pH 5	Class 3 Appropriate solubility at pH 5 and 8
Forsterite	Riebeckite	Cordierite
Wollastonite	Albite	Anorthite
Enstatite	Leucite	Glaucophane
	Spodumene	Andradite
	Jadeite	Almandine
		Nepheline
		Grossular
		Chlorite
		Tremolite
		Diopside
		Lizardite
		Fayalite

Table 7 Results of the screening methodology. Nepheline has the smallest $t_{99\%}$ and is therefore the best candidate as buffering agent.

Silicate mineral	$t_{99\%}$	Grams of mineral per mmol of PCE transformed
Nepheline	21	0.54
Fayalite	24.8	0.97
Glaucophane	29.8	0.51
Lizardite	29.8	0.45
Grossular	35	0.50
Almandine	46.8	0.74
Cordierite	48.6	0.32
andradite	53.8	0.49
Anorthite	not reached	-
Chlorite	not reached	-
Diopside	not reached	-
Tremolite	not reached	-
Enstatite	not reached	-

Figures

Fig. 1 Influence of pH on solubility of five silicate minerals (andradite, fayalite, forsterite, nepheline and wollastonite). For all these minerals, solubility decreases with increasing pH.

Fig. 2 pH versus dechlorination rate for a mixed organohalide respiring consortium. The filled diamonds represent the experimental data determined by Vainberg et al. (2009) and the line represents the fit of these data with Eq. 13.

Fig. 3 Diopside dissolution rate versus pH. The points represent the data obtained by Golubev et al. (2005) and Knauss et al. (1993). The lines were obtained by fitting these datasets to Eq. 1. For each dataset a different value of the three parameters k_{H^+}, n_{H^+} and k_W was obtained. Therefore, two values were available for each parameter. The continuous line was computed with the average value while the dotted lines were computed with the minimal and maximal values.

Fig. 4 Logarithm of mineral solubility at pH 5 (a) and pH 8 (b) for the 20 selected silicate minerals. These solubility values were calculated at 20°C in pure water. The solubility values vary by several orders of magnitude among minerals

Fig. 5 Dechlorination pattern and pH evolution for the case A (pH constant at its optimal value) (a), case B (pH inhibition) (b) and case C (introduction of 300 $m^2 l^{-1}$ of fayalite) (c).

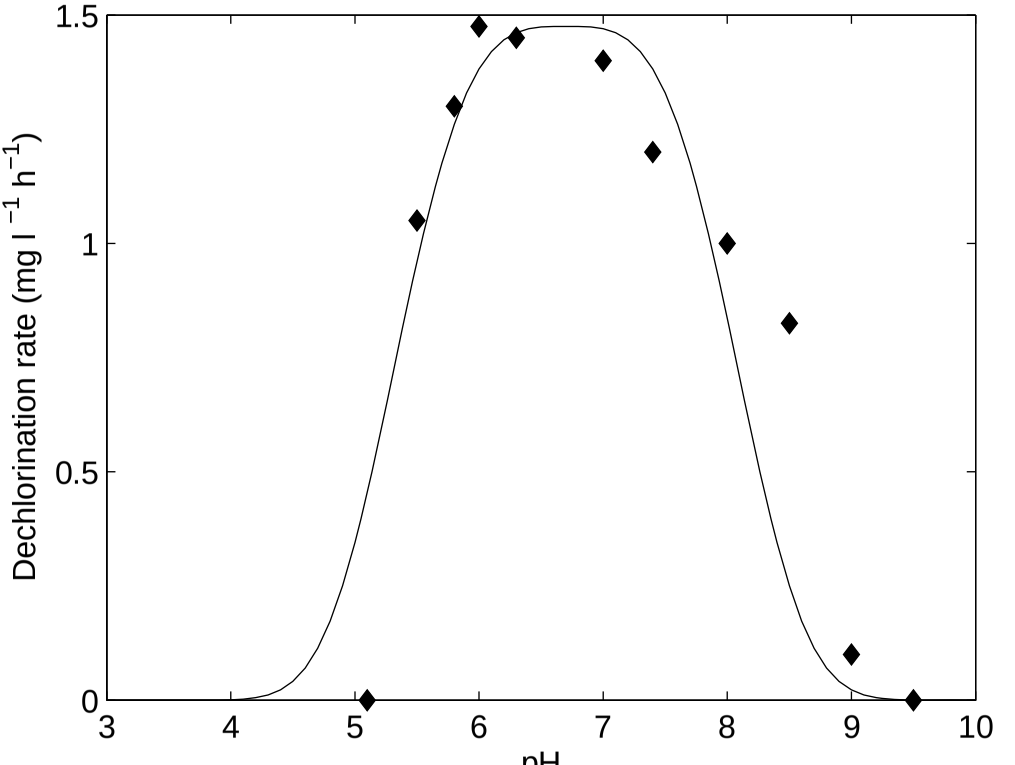
1.5
1
0.5
0
Dechlorination rate (mg l −1 h −1)
3
4
5
6
7
8
9
10
pH

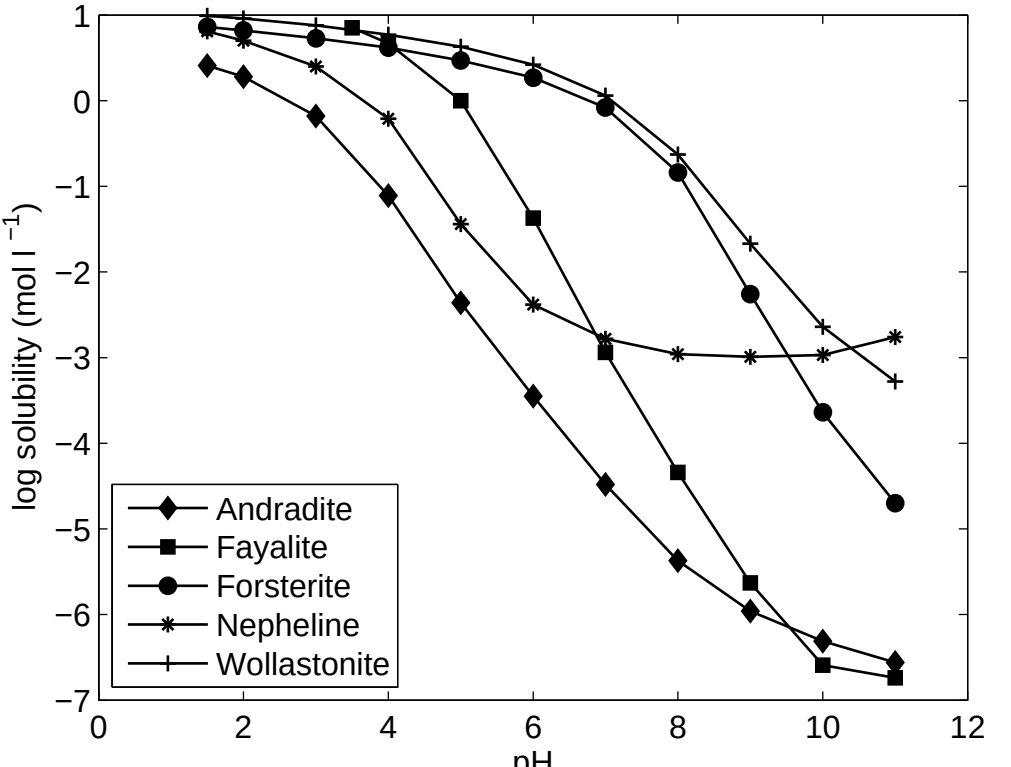
log solubility (mol l $^{-1}$)
pH
Andradite
Fayalite
Forsterite
Nepheline
Wollastonite
1
0
−1
−2
−3
−4
−5
−6
−7
0
2
4
6
8
10
12

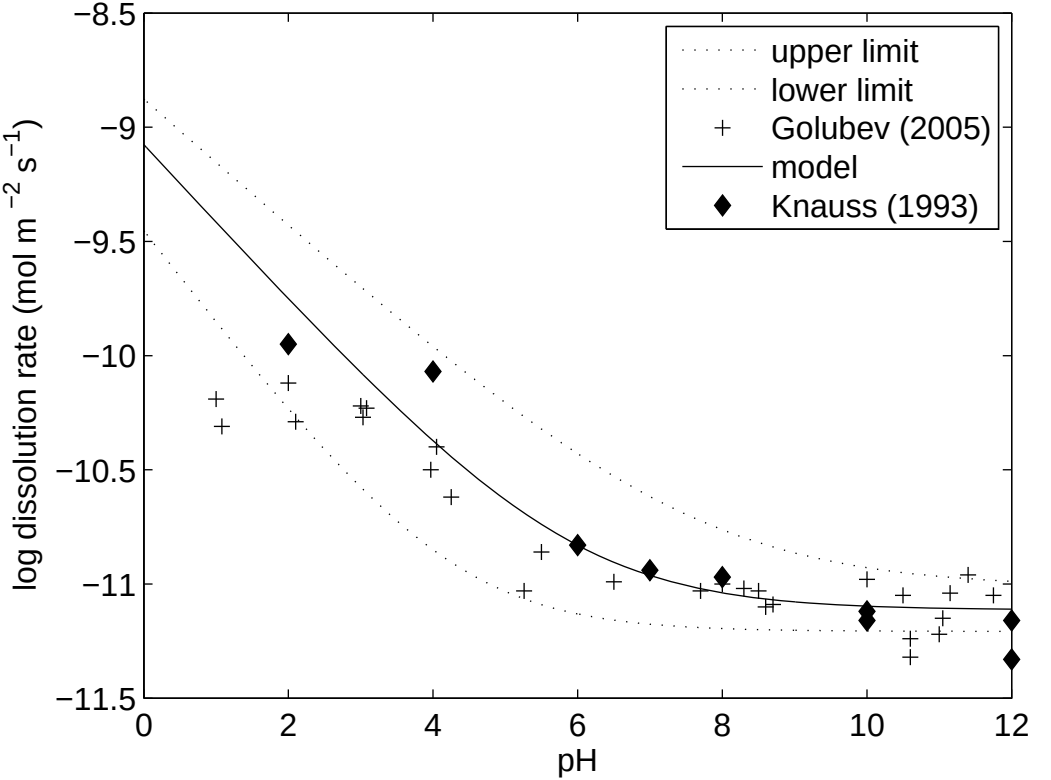
upper limit
lower limit
Golubev (2005)
model
Knauss (1993)
log dissolution rate (mol m −2 s −1)
pH
−8.5
−9
−9.5
−10
−10.5
−11
−11.5
0
2
4
6
8
10
12

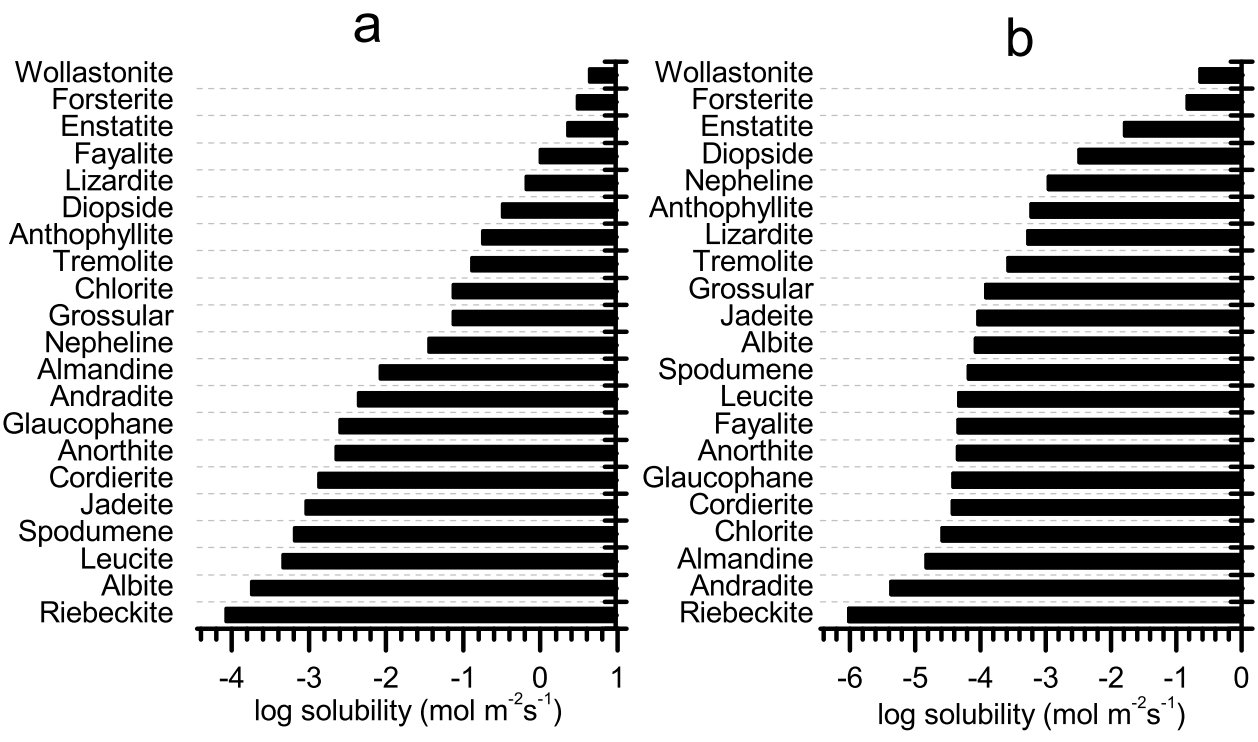
a
Wollastonite
Forsterite
Enstatite
Fayalite
Lizardite
Diopside
Anthophyllite
Tremolite
Chlorite
Grossular
Nepheline
Almandine
Andradite
Glaucophane
Anorthite
Cordierite
Jadeite
Spodumene
Leucite
Albite
Riebeckite
-4
-3
-2
-1
0
1
log solubility (mol m-2s-1)
b
Wollastonite
Forsterite
Enstatite
Diopside
Nepheline
Anthophyllite
Lizardite
Tremolite
Grossular
Jadeite
Albite
Spodumene
Leucite
Fayalite
Anorthite
Glaucophane
Cordierite
Chlorite
Almandine
Andradite
Riebeckite
-6
-5
-4
-3
-2
-1
0
log solubility (mol m-2s-1)

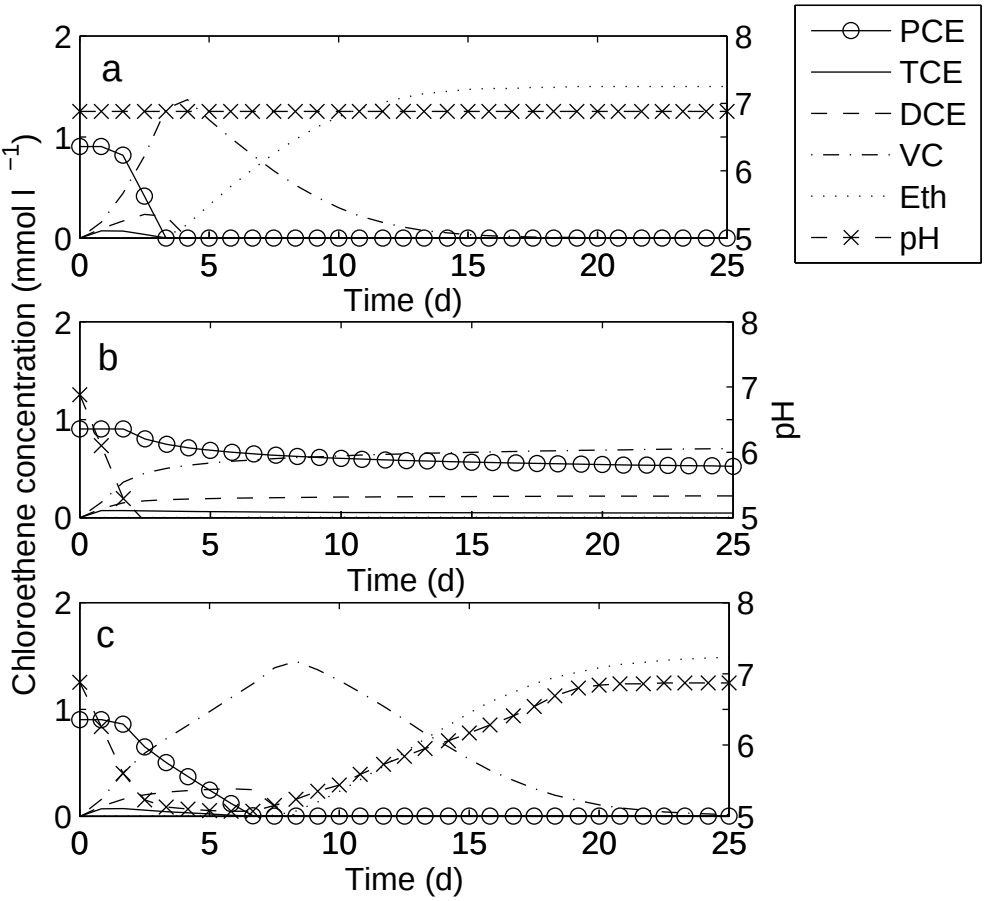
a
b
c
PCE
TCE
DCE
VC
Eth
pH
Chloroethene concentration (mmol l $^{-1}$)
pH
Time (d)
Time (d)
Time (d)
0
1
2
5
6
7
8
0
5
10
15
20
25